ACS Sustainable Chemistry & Engineering

pubs.acs.org/journal/ascecg

Research Article

Passivation of the TiO_2 Surface and Promotion of N719 Dye Anchoring with Poly(4-vinylpyridine) for Efficient and Stable Dye-Sensitized Solar Cells

Daniela F. S. L. Rodrigues, Fátima Santos, Carlos M. R. Abreu, Jorge F. J. Coelho, Arménio C. Serra,* Dzmitry Ivanou,* and Adélio Mendes

Cite This: *ACS Sustainable Chem. Eng.* 2021, 9, 5981−5990

Read Online

ACCESS | Metrics & More | Article Recommendations | Supporting Information

ABSTRACT: Dye-sensitized solar cells (DSSCs) have turned to be the most promising PV technology for indoor applications, for sustainable powering billions of IoT devices and wireless indoor sensors; DSSCs are aesthetic, cheap, and safe, and they display extremely high power conversion efficiencies (PCEs). In this study, poly(4-vinylpyridine) (P4VP) of molecular weights (MW) ranging from 2.8 to 18.5k was prepared by reversible addition-fragmentation chain transfer (RAFT) polymerization and studied as a new co-adsorbent with N719 dye to produce efficient DSSCs. P4VP adsorbs on TiO_2 via coordinative bonding to the Lewis acid centers of the titania. The adsorbed P4VP effectively hampers the back-electron recombination at the photoanode/electrolyte interface and promotes stronger covalent dye bonding. The simultaneous adsorption of P4VP with N719 allowed reaching a PCE of ca. 7.5% under 1 Sun and with almost half dye loading of the reference device. Sequential adsorption of the P4VP led to a noticeable increase of the strongly covalent bonded dye fraction making the electron injection to the titania more efficient and improving the photocurrent density. The effect of polymer MW, concentration, and adsorption sequence with the N719 on the photovoltaic performance of the DSSCs is discussed. For the first time ever, the efficient long-chain polymeric P4VP co-adsorbent rendered a device with as high PCE as 9% under 1 Sun illumination and 22.5% under indoor 1000 lx light. The PCE history under natural aging suggests that P4VP is a high-performing co-adsorbent, which allows fabrication of quite stable devices.

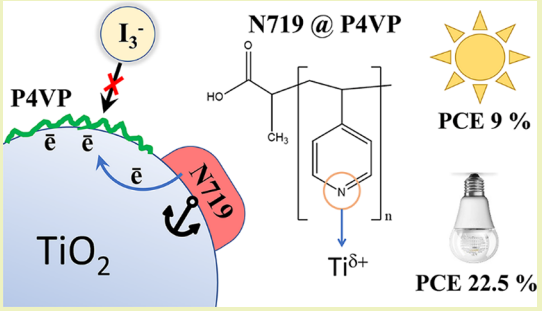

KEYWORDS: *dye-sensitized solar cells, co-adsorbents, dye-anchoring, polymers, electron recombination*

INTRODUCTION

Dye-sensitized solar cells (DSSCs) are third-generation photovoltaic devices merging fabrication simplicity, low production cost, stability, and good power conversion efficiency (PCE)[1,2] overpassing conventional Si under dim and diffused light.[3,4] Over the years, DSSCs have been extensively explored as alternatives to traditional and outdoor building-integrated photovoltaics.[5,6]

Nowadays, due to the rapid growth of the low-power-consumption electronic products, such as the Internet of Things (IoT) and wireless sensors, the development of sustainable cordless powering strategies for indoor applications became imperative turning DSSCs into a fast growing PV technology.[7] Among other photovoltaics, DSSCs are the most efficient technology for indoor use, displaying an amazingly high PCE of ca. 34%;[8,9] they can be fabricated with different true colors and aesthetically integrated into the living and working interior;[5] they are safe, in the sense that they do not contain very toxic substances such as soluble lead or tin compounds and exhibit simplicity of production. Obviously, the development of new efficient materials for high-performance DSSCs is absolutely relevant for the forthcoming commercial production.

The maximum possible PCE of DSSCs under sunlight is estimated to be 20.25%.[10] The state-of-the-art DSSCs employing Co(III)/Co(II) and Cu(II)/Cu(I) shuttles, porphyrin, and organic dyes render the PCEs ca. 13−14%,[8,11,12] and the certified record of 11.9% is still of a ruthenium dye and iodide/triiodide device.[13]

Electron back transfer to the electrolyte and the dye excited state quenching in aggregated dye molecules are among the other major hurdles for highly efficient DSSCs.[1,14] This challenge is addressed by passivating the photoanode with co-adsorbents and dye de-aggregating additives, which are introduced into the dye solution, applied after the dye has been

Received: February 5, 2021
Revised: April 1, 2021
Published: April 22, 2021

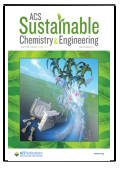

https://doi.org/10.1021/acssuschemeng.1c00842
ACS Sustainable Chem. Eng. 2021, 9, 5981−5990

adsorbed on TiO_2, or added into the electrolyte.[15] Co-adsorbents increase the PCEs of the devices improving the open circuit potential and photocurrent density, affecting the distribution and position of localized intraband gap states and suppressing electron recombination in the TiO_2/electrolyte interface.[15,16] The extensively used co-adsorbent is chenodeoxycholic acid (CDCA), a type of bile acid first identified as an efficient additive for DSSCs in 1993.[17] The effect of CDCA on the performance of DSSCs was deeply studied; CDCA became a benchmark co-adsorbent due to its exceptionally efficient TiO_2 passivation, suppression of back current, ability to prevent dye aggregation, and effect of pushing up the Fermi level of TiO_2 for enhanced charge separation.[18−22] CDCA is chemically very complex, a rather expensive compound, and dominantly produced by extraction from the animal's liver.[23] Simpler synthetic compounds were reported as effective co-adsorbents in DSSCs: 4-tertbutyl pyridine, 1-decylphosphonic acid, dineohexyl and diphenyl phosphinic acids, esters of phosphoric and carboxylic acids, and amines, among others.[15] The most studied co-adsorbents are mainly small molecules with amphiphilic bodies combined with one or few functional groups to anchor on the semiconductor: carboxylic, phosphonic, or phosphinic.

The use of long-chain molecules, i.e., the polymers, is a benefit for coating efficiently the free spaces on the mesoporous scaffold. Few studies report the polymeric co-adsorbents,[24−27] all using the benchmark N719 dye. However, attaining a reasonably high PCE was challenging. Lee et al. observed suppression of the back-electron current and downward shift of the titania conducting band edge under coordinative interaction of TiO_2 with poly(ethylene glycol); PCE was improved from 4.6 to 5.6%.[24] Carboxylic acid terminated polystyrene increased the electron lifetime by blockage of the TiO_2 surface with collapsed polymer leading to the improvement of PCE from 4.4 to 5.7%.[25] PCEs of 5.6 and 7.8% were attained by TiO_2 passivation with polymerized tetraethyl orthosilicate[26] and cross-linked methylmethacrylate/1,6-hexandiol diacrylate.[27]

In this report, carboxylic acid terminated poly(4-vinylpyridine) (P4VP) homopolymers with controlled molecular weight (MW) distribution were prepared by reversible addition-fragmentation chain transfer (RAFT) polymerization. RAFT is one of the reversible deactivation radical polymerization (RDRP) techniques that allow obtaining the polymers with controlled and narrow MW distribution.[28,29] Several P4VPs were studied as co-adsorbents with N719 dye. Adsorption of P4VP occurs mainly through the pyridinium moieties via coordination bonding of the nitrogen electron pair with Lewis acid centers of the titania. Co-adsorbed with dye, P4VP increases the charge transport resistance at the photoanode/electrolyte interface and hinders back-electron recombination and dark current. P4VP decreases dye loading when adsorbed simultaneously with N719; nevertheless, it was possible to increase the overall PCE from 5.4 to 7.5% even with 2-fold less dye adsorbed. When adsorbed sequentially after the N719, P4VP forces strong covalent bonding of the dye to TiO_2, promoting photocurrent and rendering a device with a very high PCE of 9% under standard 1 Sun illumination, surpassing the most frequently reported value of ca. 8% for the DSSCs with N719 dye.[30] The aging test suggests that P4VP allows fabricating stable devices. Under 500 and 1000 lx artificial light, the device is very favorable for efficient indoor light conversion with PCEs of 22.4 and 22.5%, respectively, compatible to that with DSSCs assembled using an expensive cobalt redox mediator.

MATERIALS AND METHODS

Poly(4-vinylpyridine) Homopolymers. Several P4VP homopolymers with different MWs of 2.8k, 3.6k, 8.5k, 13.7k, and 18.5k g mol^{-1} were synthesized by RAFT polymerization according to Scheme S1 (Supporting Information). The structure of the polymers was confirmed using ^{1}H-NMR spectroscopy (Figure S1). The synthesized polymers have a low dispersity ($Đ$) below 1.2 (Table S1, Supporting Information). The MW distribution curves obtained by size exclusion chromatography (SEC) are shown in Figure S2 (Supporting Information).

Assembly of DSSCs. DSSCs were assembled using materials, reagents, and general procedures as described elsewhere.[30] Briefly, Pt-coated FTO glasses were used as counter electrodes. Photoanodes were prepared as follows: a blocking layer with a thickness of 80 ± 5 nm was deposited by spraying a TiO_2 precursor solution on substrates heated up to 450 °C; circular-shaped photoanodes (0.13 cm^2) were formed on FTO-glasses by screen printing; 30NR-D and 18NR-AO pastes from GreatCell Solar were used to prepare a transparent mesoporous layer and to deposit a scattering opaque TiO_2 layer, with thicknesses of 21 and 7 μm, respectively. After sintering, TiO_2 films were treated with a 40 mM $TiCl_4$ aqueous solution for 20 min at 70 °C, dried, and annealed at 500 °C for 1 h. Sensitization of the mesoporous TiO_2 layer was performed using simultaneous and sequential co-adsorption of N719 dye and P4VP at *ca.* 20 ± 1 °C.

Simultaneous Co-Adsorption. The required amount of P4VP was added into 0.3 mM N719 dye solution in absolute ethanol and stirred for *ca.* 1 h to complete the polymer dissolution. Mesoporous TiO_2 films on FTO-coated glasses were immersed in the as-prepared solution and kept for 24 h. Sensitization of the TiO_2 for the reference devices followed the same procedure using the dye solution without the addition of P4VP.

Sequential Adsorption. First, the dye was adsorbed on the mesoporous TiO_2 layer from a 0.3 mM solution of N719 in absolute ethanol for 24 h. Then, the TiO_2 layer with adsorbed dye was immersed into P4VP ethanol solution for 12 ± 2 h. Photoanodes for reference devices were produced by immersing the TiO_2 layer with preadsorbed dye in absolute ethanol without polymer for 12 ± 2 h.

After sensitization, the photoanodes were rinsed with absolute ethanol, dried under N_2 flow, and immediately used to assemble the devices. A commercial EL-HPE iodine electrolyte based on an acetonitrile/valaronitrile solvent mixture was purchased from GreatCell Solar. For typical composition of the electrolyte, interested readers may consult ref 15 in our previous study.[30]

The adsorbed concentration of the dye on the mesoporous TiO_2 layer was determined as described elsewhere.[31]

Characterization. The current vs applied potential (I−V) response of the cells was recorded using a Zennium (Zahner) electrochemical station at temperature 20 ± 1 °C. A Solar Simulator MiniSol (LSH-7320, Newport) was used to illuminate the devices (AM1.5G, 100 mW cm^{-2}). The illumination light was calibrated with a Si reference cell. An LED lamp (Osram, Class A+, 60 W, 2700 K) was used as an artificial interior light source. Power of the light (W·m^{-2}) derived by the lamp was determined with a radiometer Delta Ohm HD 2102.2. The electrochemical impedance spectra were collected in the dark at a potential of 20 mV below the open-circuit potential of the DSSCs, and a sinusoidal perturbation with a peak-to-zero amplitude of 10 mV in the frequency range of 100 kHz to 0.1 Hz was applied using an Autolab (PGSTAT 302 N, Metrohm). The impedance spectra were analyzed using the ZView software.

Absorption spectra were collected using a Shimadzu UV-3600 spectrometer. The infrared spectra were recorded using a VERTEX 70 FTIR spectrometer (Bruker) in transmittance mode with a high-sensitivity DLaTGS detector at room temperature. Samples were measured in ATR mode, with a A225/Q Platinum ATR Diamond crystal with a single reflection accessory. The spectra were recorded from 4000 to 500 cm^{-1} with a resolution of 4 cm^{-1}.

https://doi.org/10.1021/acssuschemeng.1c00842
ACS Sustainable Chem. Eng. 2021, 9, 5981−5990

RESULTS AND DISCUSSION

Adsorption of P4VP and N719 Dye on TiO_2. For the sensitization of photoanodes, N719 dye and P4VP were adsorbed on the mesoporous TiO_2 layer in two different ways: simultaneously and sequentially. The concentration of the dye in the solution was fixed, and the concentration of the added P4VP was varied from 3 to 75 μM. It will be later shown that among the P4VPs studied, the polymer with a MW of 8500 (denoted as 8.5k) at a concentration of 30 μM in co-adsorbing solution allows obtaining the most efficient DSSCs. For convenience, further discussion is centred in the P4VP-8.5k polymer and the effect of the polymer MW will be discussed later. Figure 1a shows the adsorbed dye loading in the TiO_2 layer using the two adsorption procedures: co-adsorption and sequential adsorption.

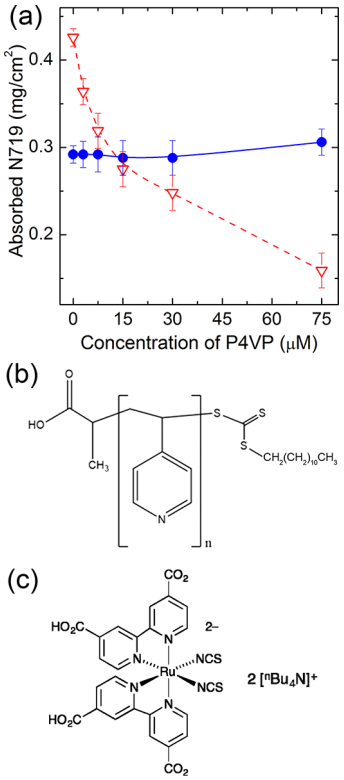

Figure 1. Adsorbed dye loading in the TiO_2 layer vs P4VP-8.5k concentration in the solution for simultaneous (empty triangles) and sequential (solid circles) adsorption (a). Molecular structures of the P4VP produced (b) and N719 dye (c).

During simultaneous adsorption, the amount of adsorbed dye drops exponentially as the polymer concentration increases in the solution. The drop of the dye adsorption indicates that P4VP effectively competes with the dye for the surface sites of titania. The dye anchors to TiO_2 through the carboxylic groups (Figure 1c).[32,33] The adsorption of P4VP on titania is based on the terminal carboxylic group (Figure 1b) and the pyridine heterocycle[34,35] of the polymer repeating side group. In simultaneous adsorption mode, the molar concentration of the added P4VP is *ca.* 10 times less than that of the dye, causing a drastic decrease of the dye loading. Considering that each P4VP molecule contains *ca.* 77 pyridine moieties to each terminal carboxylic group, it is easy to conclude that the adsorption of P4VP on TiO_2 occurs mainly via the pyridine heterocycles. The FTIR spectra presented in Figure 2 evidence the adsorption of P4VP on TiO_2. Also, pyridine is an organic

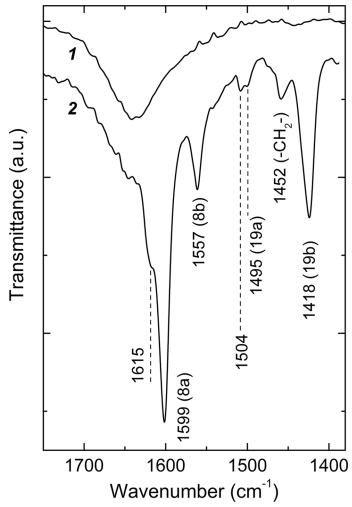

Figure 2. FTIR spectra of the pristine TiO_2 (*1*) and after 12 h of immersion in 30 μM P4VP-8.5k solution in ethanol (*2*).

base that can form a salt with the carboxylic group of N719, hindering the interaction between this group and the TiO_2 surface.

For the pristine mesoporous titania layer, the broad absorption peak at *ca.* 1640 cm^{-1} is associated with the O–H vibrations due to the chemically and physically adsorbed water on the surface of TiO_2 nanoparticles.[36,37] After the immersion of TiO_2 in an ethanolic solution of P4VP, five characteristic bands of P4VP appear in the FTIR spectrum in the frequency range of 1400–1700 cm^{-1}. The band at 1452 cm^{-1} was assigned to the planar deformation vibration of the $-CH_2-$ groups in the polymer chain.[38] The other four absorption bands at 1599, 1557, 1495, and 1418 cm^{-1} were assigned to 8a, 8b, 19a, and 19b in-plane vibrational modes of the pyridine ring.[34,39] The positions of these bands match the characteristic frequencies of the pyridine moiety in the structure of P4VP.[38] Owing to the lone pair of the nitrogen atom, adsorption of pyridine moieties of the P4VP on titania can occur both on the Lewis acid (exposed Ti^{n+} cation) or on Brønsted acid (surface-bonded hydroxyls) centers of the oxide. Also, the formation of hydrogen-bonded complexes with titania surface hydroxyls could not be ruled out.[34,40] For pyridine adsorbed on metal oxides, vibration modes 8a and 19b are the most sensitive to the nature of interactions involving the lone pair of nitrogen; both vibrational modes exhibit high-frequency shifts when the electron pair is donated.[39] The pronounced shoulder observed in the IR spectra at 1615 cm^{-1} is within the frequency range for vibration mode 8a that is typically observed for hydrogen-bonded pyridine (1590–1614 cm^{-1}) or for coordinatively bonded Lewis acid site pyridine (1600–1635 cm^{-1}).[41] Adsorption of P4VP on TiO_2 via hydrogen bonding would not cause such a significant decrease in the dye loading (Figure 1) as the hydrogen bond energy (few kJ mol^{-1}) is much lower than the energy of N719 dye adsorption on TiO_2 – *ca.* 190.8 kJ mol^{-1}.[42] Consequently, the adsorption of P4VP on TiO_2 should be owed to pyridine moiety bonding with Lewis acid sites at the titania surface. The vibration mode 19b is not shifted, more likely because the pyridinium ring stretch

https://doi.org/10.1021/acssuschemeng.1c00842
ACS Sustainable Chem. Eng. 2021, 9, 5981–5990

vibration is affected by the polymer chain. A similar pattern in the IR spectra was observed under the formation of P4VP complexes with strong Lewis acids like Cu(II),[43] Pd(II),[44] and Ru(II)[45] ions. The band at 1504 cm^{-1} in the IR spectra belongs to the vibrational mode 19a, which tends to exhibit two bands when the intermolecular pyridine−pyridine interactions are weakened.[39] The adsorption of P4VP on titania likely leads to the reorganization of pyridinium fragments so that the accessibility of rotational transitions is improved, leading to two bands of the vibrational mode 19a.

Under sequential adsorption of N719 and P4VP, dye loading in TiO_2 remains constant regardless of the concentration of the polymer in the solution (Figure 1a). Dye anchoring to TiO_2 through the carboxylic group is much stronger than P4VP binding to TiO_2 through pyridine moieties[46] ensuring no dye desorption under exposure to P4VP solution. Nevertheless, in sequential adsorption, P4VP is attached to the titanium dioxide surface with preloaded dye as the FTIR spectra presented in Figure 3 confirm.

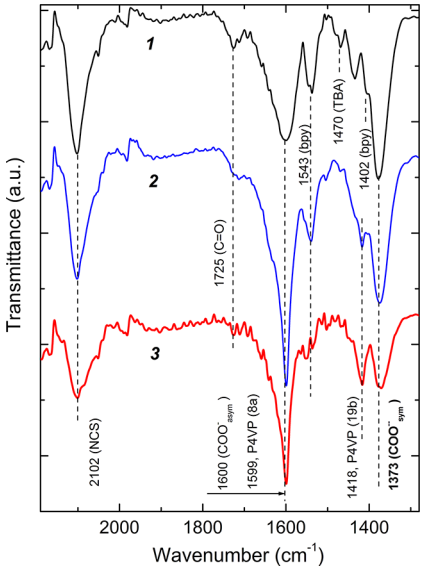

Figure 3. FTIR spectra of TiO_2 after adsorption of N719 dye solely (*1*), N719 dye with P4VP-8.5k (30 μM) sequentially (*2*), and simultaneously (*3*).

The interaction of N719 and TiO_2, the exact anchoring mechanism of the dye, has been debated for decades. FTIR spectroscopy is commonly used to identify the possible mechanism of dye anchoring via monitoring the vibration response from the functional groups constituting dye molecules.[32,47,48]

The IR spectrum of the N719 dye on anatase titania shows distinctive absorption bands of the NCS group (2100 cm^{-1}), carbonyl C=O (1725 cm^{-1}), asymmetric vibration of COO^-_{asym} (1600 cm^{-1}), C=C in bpy (1543 cm^{-1}), TBA ion (1470 cm^{-1}), bpy (1402 cm^{-1}), and symmetric vibration of COO^-_{sym} (1373 cm^{-1}). Transformations of the signature of these groups in the IR spectra are related to the peculiarities of N719 dye anchoring to titania, profoundly reviewed and explored elsewhere.[47] Briefly, the impact of the NCS group on dye anchoring to TiO_2 is minor in most cases, but if it happens, courses as a large shift (*ca.* 10 cm^{-1}) of the NCS band toward lower wavenumbers and the band intensity becomes significantly reduced;[32] strong anchoring through carboxylic and carboxylate groups is monitored with a decrease of the intensity of C=O vibration and the appearance of asymmetric and symmetric stretching bands of COO^-; the latter band evidences the covalent bonding to TiO_2. Consequently, the relative amount of bound dye to the titania surface can be estimated by the relative intensities of the C=O band and COO^-_{sym}; TBA vibrational modes are not active in the spectrum in the case of both carboxylate anions of N719, which are covalently bonded to TiO_2.[47]

Under sequential adsorption with P4VP, the band corresponding to vibrational mode 19b is observed in the IR spectra while the band 8a of P4VP overlaps with the COO^-_{asym} making this band stronger (Figures 3 and 2). More important, vibrations of carbonyl C=O are weakened, and the TBA band tends to vanish. This transformation of the spectrum may evidence the appearance of new anchoring bonds between the dye and titania,[48] i.e., the dye displays a stronger bond after treating with P4VP. When dye N719 becomes strongly bonded, a blue shift of the optical band assigned to metal-to-ligand charge transfer is observed;[32] this blue shift is indeed observed in Figure 4. For the dye loaded on TiO_2, an

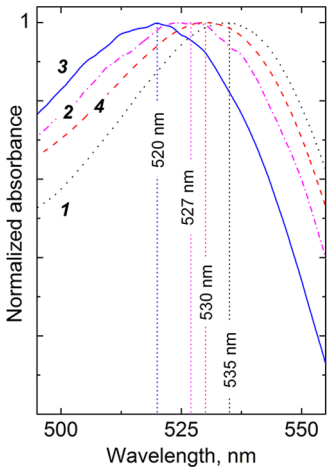

Figure 4. Normalized absorption spectra of the TiO_2 layer right after adsorption of N719 dye (*1*) and after 12 h of immersing in ethanol (*2*); after sequential (*3*) and simultaneous (*4*) adsorption of the dye with P4VP-8.5k.

absorption maximum at 535 nm shifts to 520 nm after exposure to P4VP solution, wherein after the exposure to ethanol solution without P4VP, it shifts only to 527 nm.

After simultaneous co-adsorption, the intensities of characteristic bands of the dye (NCS, bpy, and COO^-_{sym}) are weaker as less dye is adsorbed (Figure 1). The bands corresponding to C=O and TBA vibrations mostly disappear. The position of the NCS band is not affected; therefore, its intensity can be used to estimate the relative amount of adsorbed dye. Relative to the intensity of the NCS band, band 19b of P4VP at 1418 cm^{-1} is more pronounced than those in previous cases, indicating that more polymer is adsorbed on the surface. Another distinguishing feature is a small intensity of the band assigned to covalent dye binding to TiO_2, i.e., the COO^-_{sym} band is less intense than the NCS band. It points out that the anchoring of N719 is affected and weakened when P4VP is added to the sensitizing solution. Besides, the absorption band of N719 at 535 nm is mostly not affected. When P4VP and N719 dye are both in the sensitization solution, pyridinium

https://doi.org/10.1021/acssuschemeng.1c00842
ACS Sustainable Chem. Eng. 2021, 9, 5981−5990

moieties may react as Brønsted base with dye carboxylic groups causing deprotonation. As a result, less dye in the deprotonated form is bonded to the anatase surface.[33]

Effect of Co-Adsorbed P4VP on the Photovoltaic Performance of DSSCs. Figure 5 presents a set of photocurrent−potential responses of the DSSCs assembled using photoanodes with co-adsorbed P4VP-8.5k and N719 dye.

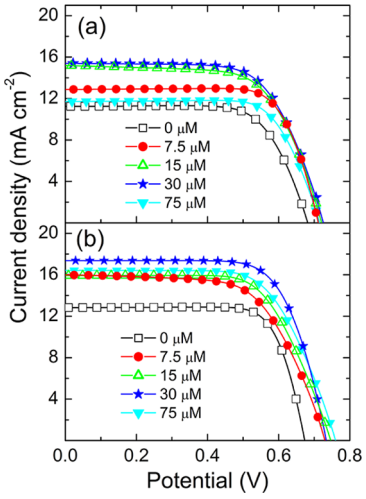

Figure 5. *I*−*V* curves of the DSSCs produced using simultaneous (a) and sequential (b) adsorption of N719 and P4VP-8.5k.

The devices prepared using both protocols of P4VP co-adsorption with N719 display *I*−*V* curves characteristic of a photodiode. For the wide range of concentrations of the P4VP added to the co-adsorbing solutions, from 7.5 to 75 μM, the photocurrent densities and V_{OC}s of these devices largely surpass those of the reference cells. For the convenience of the discussion, the main photovoltaic parameters (J_{SC}, V_{OC}, FF, and PCE) of the DSSCs were calculated from the *I*−*V* response and are plotted in Figure 6.

The highest 1 Sun PCE improvement occurs for a polymer concentration of 30 μM: from 5.4% of the reference cell to 7.5% and from 6.5% of the reference cell to 9% with P4VP, in simultaneous and sequential adsorption, respectively. It is noteworthy here that based on N719 dye devices produced using conventional CDCA, the co-adsorbent may allow as high PCE as 9.5% when thoroughly optimized;[31] in this study, devices with CDCA displayed 8% in average of three cells showing the promise of the P4VP co-adsorbent.

In the cells prepared by simultaneous co-adsorption, J_{SC} peaks for the P4VP concentration in the solution of 30 μM are shown (Figure 6b), although the amount of loaded dye in TiO_2 is much less than that in the reference device (Figure 1). Adsorbed polymer suppresses the back-electron recombination and leads to a J_{SC} increase even at low dye loadings. A high FF ca. 0.7 (Figure 6d) was achieved for all the devices. At P4VP concentrations above 30 μM, a drop in J_{SC} is observed; this drop was assigned to a substantial decrease in the amount of adsorbed dye (Figure 1).

The devices with a 1 Sun PCE of 9% were characterized under artificial light (Figure 7).

Power generation under indoor light with the use of DSSCs is a relatively new trend, and no standard indoor-light source has been established so far.[49] We used a typical LED source

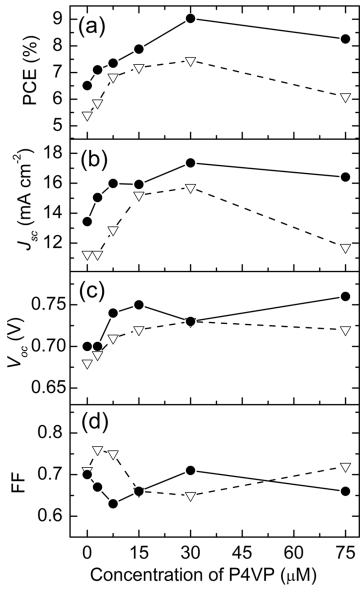

Figure 6. Photovoltaic parameters: PCE (a), J_{SC} (b), V_{OC} (c), and FF (d) of the DSSCs vs concentration of the P4VP-8.5k in the solutions for simultaneous (empty triangles) and sequential (filled circles) co-adsorption with N719.

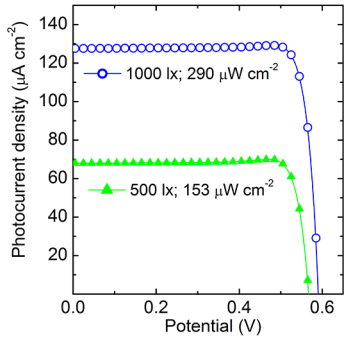

Figure 7. *I*−*V* curves of the DSSCs under different intensities of the artificial light delivered from an LED lamp.

with intensities of 500 and 1000 lx and incident light powers of 153 and 290 μW·cm^{-2}, respectively. The PCE was calculated from the ratio of the maximum power produced by the DSSC to the incident light power. The cells display reproducible *I*−*V* responses with maximum output powers of 34.2 and 65.3 μW cm^{-2} and PCEs of 22.4 and 22.5% under 500 and 1000 lx, respectively. It is noteworthy that the output power and PCE under artificial light of the obtained devices are compatible and, in most cases, surpass counterparts with an expensive cobalt electrolyte and untrivial dyes, reviewed elsewhere.[9] The reason for that has been recently clearly stated by the authors.[30] Amazingly high PCE under artificial light with N719 dye and iodine electrolyte was attained due to the perfect match of the dye quantum yield spectrum with the incident light, proper optimization of the photoanode structure, and efficient strategy for suppression of back electron recombination.

For sequential adsorption, the N719 loading in TiO_2 is approximately constant regardless of the P4VP concentration in the solution. It is noteworthy that photocurrent from the photoanodes sensitized by sequential adsorption always surpasses that obtained by simultaneous co-adsorption (Figure

https://doi.org/10.1021/acssuschemeng.1c00842
ACS Sustainable Chem. Eng. 2021, 9, 5981−5990

6b), even for the cases when the amount of loaded dye is higher, i.e., for P4VP concentration below 15 μM (Figure 1). Two reasons were proposed for J_{SC} improvement under sequential adsorption with P4VP: (i) suppression of the back-electron recombination by the adsorbed polymer; (ii) stronger dye anchoring after P4VP treatment (Figure 4).

Under P4VP co-adsorption V_{OC} tends to increase more after the sequential procedure (Figure 6c). Suppressed dark current originates from the improvement of the V_{OC} (Figure 8).

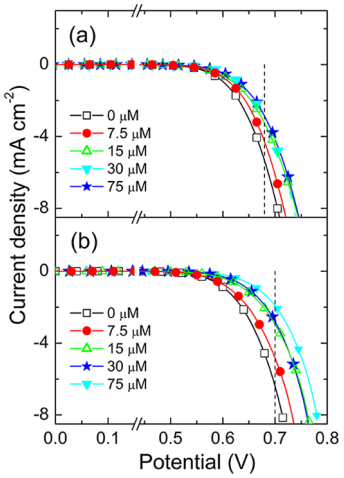

Figure 8. Polarization curves recorded in the dark for DSSCs prepared with photoanodes sensitized via simultaneous (a) and sequential (b) adsorption of dye N719 and P4VP-8.5k at different concentrations. Vertical dotted lines point the V_{OC} of the devices assembled without P4VP.

At potentials close to V_{OC}, the dark current produced by the cells without photoanode passivation is relatively high, *ca.* −5.4 and −6.6 mA·cm^{-2} for the references used in simultaneous and sequential sensitization procedures, respectively (Figure 8). After the adsorption of P4VP, the dark current is *ca.* 2 times suppressed, rendering the V_{OC} as high as 0.73 V for the best-performing devices (Tables S2 and S3 in the Supporting Information).

The suppression of the dark current is related to the increased resistance at the photoanode/electrolyte interface; the EIS analyses of the cells corroborate this (Figure 9). The Nyquist plots in Figure 9 show the EIS response at V_{OC} (forward bias in the dark) of the DSSCs with photoanodes prepared by simultaneous and sequential adsorption of the dye and P4VP; two capacitive semicircles can be seen.

The small and large capacitive semicircles are associated with electron transport at the interfaces of the counter electrode/electrolyte and of the photoanode/electrolyte, respectively. Increasing the concentration of P4VP in the solution enlarges the capacitive loop displayed by the photoanode/electrolyte interface; the charge transport resistance at the interface becomes higher. This resistance is normally assigned to the back-electron recombination reaction with triiodide.[50] For estimating the numerical values of interfacial charge transport resistances, the EIS spectra were fitted using a simplified equivalent circuit (Figure 9c). Constant phase elements CPE_{FTO} and CPE_{CE} stand for FTO/electrolyte and counter electrode/electrolyte interfaces, respectively; charge transfer resistances R_S, R_{CE}, and R_K are related to series resistance, counter electrode/electrolyte, and

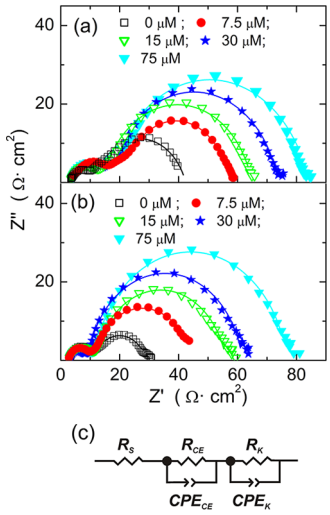

Figure 9. Nyquist plots obtained from DSSCs with photoanodes sensitized via simultaneous (a) and sequential (b) adsorption of P4VP. Solid lines stand for the fits of EIS data to the equivalent circuit (c).

photoanode/electrolyte interfaces, respectively. Table 1 summarizes the fitting parameters of the equivalent model.

Table 1. Resistances of the Cells (in Ω cm^2) Obtained by Fitting the Model to Nyquist Plots

concentration of P4VP (μM)	simultaneous			sequential		
	R_S	R_{CE}	R_K	R_S	R_{CE}	R_K
0	2.8	9.3	30.24	2.9	8.2	18.0
3	3.2	11.6	35.3	2.7	6.3	19.1
7.5	2.8	18.1	37.4	2.5	8.6	33.5
15	3.1	11.6	50.0	2.8	9.0	44.2
30	3.0	14.2	56.5	2.7	6.6	52.4
75	3.4	14.0	66.6	2.8	8.6	65.4

Resistance R_K gradually increases with the polymer concentration, while resistances R_S and R_{CE} are mostly constant. The effective suppression of the back-electron recombination by P4VP originates from higher photocurrents (Figure 5, Figure 6b); for the case of simultaneous co-adsorption, this phenomenon happens even at low N719 loads (Figure 1). It should be emphasized that the dye load remains approximately constant during sequential adsorption. Still, at high concentrations of P4VP in the solution, the photocurrent drops (Figure 6b, 75 μM), although R_K is high. This phenomenon was assigned to the dye regeneration hindering due to the excessive adsorption of P4VP. Low photocurrent at high R_K points that P4VP adsorbs not only on the TiO_2 surface but also on the dye layer.

Figure 10 presents the effect of the MW of P4VP on the photovoltaic parameters of the devices prepared with a polymer concentration of 30 μM. This concentration of P4VP allows producing the best-performing devices. Metrics of the DSSCs obtained in the range of P4VP concentrations from 3 to 75 μM for P4VPs with different MWs of 2.8k, 3.6k, 8.5k, 13.7k, and 18.5k are summarized in Tables S2 and S3 and visualized in Figure S4 in the Supporting Information.

Using P4VPs with MWs of 2.8k and 3.6k as co-adsorbents allows obtaining slightly higher values for the photocurrent and

https://doi.org/10.1021/acssuschemeng.1c00842
ACS Sustainable Chem. Eng. 2021, 9, 5981−5990

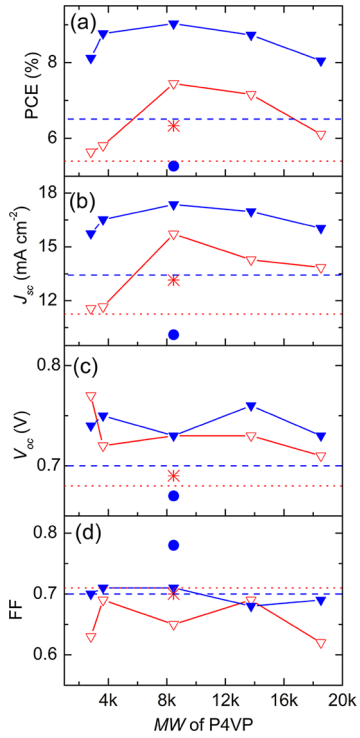

Figure 10. Photovoltaic metrics: PCE (a), J_{SC} (b), V_{OC} (c), and FF (d) of the DSSCs with photoanodes sensitized by simultaneous (empty triangles) and sequential (filled triangles) co-adsorption at a fixed concentration of the polymer (30 μM) vs the MWs of the P4VPs. Standalone points show parameters of the DSSCs assembled using 2.3 mM 4-ethylpyridine in solutions for simultaneous (red stars) and sequential (blue circles) co-adsorption. Horizontal lines guide the eyes for the metrics of reference devices for simultaneous (red dotted line) and sequential (blue dashed line) adsorption procedures.

for the PCE than for the reference cells, and the P4VP with a MW of 8.5k produced the best-performing devices (Figure 10). Polymers with a MW above 8.5k led to a further drop of the PCE, mainly due to losses in the current density. The photocurrent decrease is caused by the excessive adsorption of the polymer when P4VP displays long chains, 127 and 173 pyridinium fragments in P4VPs with MWs of 13.7k and 18.5k, respectively. An excess of the polymer either hinders dye regeneration when the P4VP has been adsorbed after dye loading or prevents dye adsorption when the polymer is adsorbed simultaneously with the dye. P4VP-8.5k, with *ca.* 77 fragments of pyridine, produced the highest photocurrent by balancing the suppression of the back-electron recombination and the dye regeneration.

Besides the very high 1 Sun PCE of *ca.* 9% and decent PCE under artificial light ca. 22.5%, it is essential to emphasize the role of the polymeric structure of the co-adsorbent and the need for thorough tuning its concentration in the solution. Using a substance mimicking the repeating unit, namely, 4-ethylpyridine, at the concentration equal to the overall concentration of the pyridine fragments in the polymer, which is equivalent to a 2.3 mM solution, did not lead to such a high PCE (Figure 10). Another example is the use of P4VPs with a MW of ca. 18.5k; to reach the same amount of pyridine units in the solution, the concentration of the polymer should be *ca.* 2.2 times less than the concentration of the P4VP-8.5k. At this concentration, P4VP-18.5k does not produce a PCE as high as for P4VP-8.5k (Tables S2 and S3, Figure S3, Supporting Information). To understand the effect of the polymer chain length on the adsorption and related DSSC performance, more detailed studies on solvent−polymer−dye−TiO_2 interactions should be addressed in the future.

Long-term stability is crucial for photovoltaic device applications. The history of the PCE of the best-performing devices produced using sequential adsorption of P4VP-8.5k (30 μM) and dye was followed during 300 h under natural aging (Figure 11). Initially, the PCE slightly increased, which is typical behavior of DSSCs,[51] and then stabilized after *ca.* 100 h of aging.

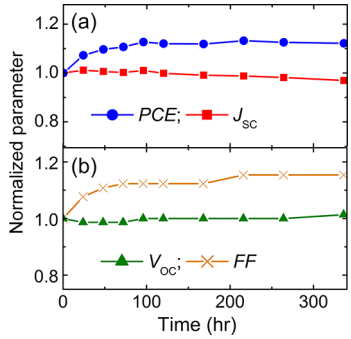

Figure 11. History of the PCE and J_{SC} (a), and V_{OC} and FF (b) for DSSCs with a 30 μM P4VP-8.5k co-adsorbent.

During the aging period, J_{SC} and V_{OC} remained mostly constant, while the FF slightly increased. The observed history of the photovoltaic parameters suggests that P4VP is a very promising and advantageous co-adsorbent for the fabrication of stable devices.

CONCLUSIONS

P4VP homopolymers are disclosed as favorable co-adsorbents for the sensitization of photoanodes to produce efficient DSSCs. P4VP adsorbs on the TiO_2 surface preferentially via pyridine moieties by donating a nitrogen lone electron pair to Lewis acid sites on the titania surface. Co-adsorption with N719 dye and P4VP effectively suppresses back-electron recombination and hinders dark current, improving photocurrent density, V_{OC}, and PCE. When the dye and P4VP are adsorbed from a solution simultaneously, the effective competition for the TiO_2 surface is accompanied by dye deprotonation under pyridinium Brønsted base, reduces the fraction of the strongly covalent-bonded dye, and causes exponential decrease of the dye loading on the TiO_2 surface. Nevertheless, even with almost half of the loaded dye amount, the effective surface passivation under P4VP benefited to an overall PCE of 7.5%, surpassing the reference devices with a PCE of 5.4% under 1 Sun illumination.

When co-adsorbed sequentially after the dye, P4VP did not cause dye desorption and led to a higher fraction of the strongly covalent bonded N719 dye. The latter, combined with effective suppression of the back recombination, led to a significant increase of electron injection efficiency from the excited dye to titania, allowing high photocurrent densities and open circuit potentials. For the first time ever, the use of the polymeric P4VP co-adsorbent sequentially co-adsorbed with N719 dye rendered a device displaying a PCE as high as 9% under 1 Sun illumination and 22.5% under 1000 lx artificial light and fully stable. The use of a cheap fully synthetic P4VP

https://doi.org/10.1021/acssuschemeng.1c00842
ACS Sustainable Chem. Eng. 2021, 9, 5981−5990

co-adsorbent instead of an expensive animal-derived CDCA is beneficial for reducing the price of a future commercial product.

■ ASSOCIATED CONTENT

Supporting Information

The Supporting Information is available free of charge at https://pubs.acs.org/doi/10.1021/acssuschemeng.1c00842.

Procedure and conditions for poly(4-vinylpyridine) homopolymer synthesis, 1H-NMR spectra of the P4VPs, SEC chromatograms of the P4VPs with different molecular weights, photovoltaic parameters of the DSSCs produced with the P4VP co-adsorbent, PCEs of the DSSCs vs concentration of the P4VPs with different MWs used for simultaneous and sequential co-adsorption (PDF)

■ AUTHOR INFORMATION

Corresponding Authors

Arménio C. Serra − *Centre for Mechanical Engineering, Materials and Processes, Department of Chemical Engineering, University of Coimbra, 3030-790 Coimbra, Portugal;* orcid.org/0000-0001-8664-2757; Email: armenio.serra@gmail.com

Dzmitry Ivanou − *LEPABE, Departamento de Engenharia Química, Faculdade de Engenharia, Universidade do Porto, 4200-465 Porto, Portugal;* orcid.org/0000-0002-5313-4016; Email: ivanou@fe.up.pt

Authors

Daniela F. S. L. Rodrigues − *Centre for Mechanical Engineering, Materials and Processes, Department of Chemical Engineering, University of Coimbra, 3030-790 Coimbra, Portugal;* orcid.org/0000-0002-1969-2962

Fátima Santos − *LEPABE, Departamento de Engenharia Química, Faculdade de Engenharia, Universidade do Porto, 4200-465 Porto, Portugal*

Carlos M. R. Abreu − *Centre for Mechanical Engineering, Materials and Processes, Department of Chemical Engineering, University of Coimbra, 3030-790 Coimbra, Portugal;* orcid.org/0000-0003-0888-7630

Jorge F. J. Coelho − *Centre for Mechanical Engineering, Materials and Processes, Department of Chemical Engineering, University of Coimbra, 3030-790 Coimbra, Portugal;* orcid.org/0000-0001-9351-1704

Adélio Mendes − *LEPABE, Departamento de Engenharia Química, Faculdade de Engenharia, Universidade do Porto, 4200-465 Porto, Portugal;* orcid.org/0000-0003-2472-3265

Complete contact information is available at: https://pubs.acs.org/10.1021/acssuschemeng.1c00842

Notes

The authors declare no competing financial interest.

■ ACKNOWLEDGMENTS

D.F.S.L.R. acknowledges the FCT − Fundação para a Ciência e a Tecnologia, for the doctoral grant SFRH/BD/131818/2017. This research is sponsored by FEDER funds through the program COMPETE − Programa Operacional Factores de Competitividade − and by national funds through FCT − Fundação para a Ciência e a Tecnologia, under the project UIDB/00285/2020. NMR data was collected at the UC-NMR facility, which is supported in part by FEDER − European Regional Development Fund through the COMPETE Programme (Operational Programme for Competitiveness) and by National Funds through FCT − Fundação para a Ciência e a Tecnologia (Portuguese Foundation for Science and Technology) through grants REEQ/481/QUI/2006, RECI/QEQ_QFI/0168/2012, CENTRO-07-CT62-FEDER-002012, and Rede Nacional de Ressonância Magnética Nuclear (RNRMN). C.M.R.A. wishes to thank Fundação para a Ciência e a Tecnologia (FCT) through the Scientific Employment Stimulus 2018 (CEECIND/03591/2018) for the financial support. F.S. acknowledges FCT doctoral grant SFRH/BD/132388/2017. Base Funding UIDB/00511/2020 of the LEPABE through the FCT/MCTES (PIDDAC). Projects PTDC/EQU-EQU/30510/2017 - POCI-01-0145-FEDER-030510 (Sunflow); SunStorage - POCI-01-0145-FEDER-016387.

■ REFERENCES

(1) Sharma, K.; Sharma, V.; Sharma, S. S. Dye-Sensitized Solar Cells: Fundamentals and Current Status. *Nanoscale Res. Lett.* **2018**, *13*, 381−427.

(2) Mariotti, N.; Bonomo, M.; Fagiolari, L.; Barbero, N.; Gerbaldi, C.; Bella, F.; Barolo, C. Recent Advances in Eco-Friendly and Cost-Effective Materials towards Sustainable Dye-Sensitized Solar Cells. *Green Chem.* **2020**, *22*, 7168−7218.

(3) Toyoda, T.; Sano, T.; Nakajima, J.; Doi, S.; Fukumoto, S.; Ito, A.; Tohyama, T.; Yoshida, M.; Kanagawa, T.; Motohiro, T.; Shiga, T.; Higuchi, K.; Tanaka, H.; Takeda, Y.; Fukano, T.; Katoh, N.; Takeichi, A.; Takechi, K.; Shiozawa, M. Outdoor Performance of Large Scale DSC Modules. *J. Photochem. Photobiol., A* **2004**, *164*, 203−207.

(4) Cornaro, C.; Bartocci, S.; Musella, D.; Strati, C.; Lanuti, A.; Mastroianni, S.; Penna, S.; Guidobaldi, A.; Giordano, F.; Petrolati, E.; Brown, T. M.; Reale, A.; Di Carlo, A. Comparative analysis of the outdoor performance of a dye solar cell mini-panel for building integrated photovoltaics applications. *Progr. Photovolt.: Res. Appl.* **2015**, *23*, 215−225.

(5) Fakharuddin, A.; Jose, R.; Brown, T. M.; Fabregat-Santiago, F.; Bisquert, J. A Perspective on the Production of Dye-Sensitized Solar Modules. *Energy Environ. Sci.* **2014**, *7*, 3952−3981.

(6) Saifullah, M.; Gwak, J.; Yun, J. H. Comprehensive review on material requirements, present status, and future prospects for building-integrated semitransparent photovoltaics (BISTPV). *J. Mater. Chem. A* **2016**, *4*, 8512−8540.

(7) Mathews, I.; Kantareddy, S. N.; Buonassisi, T.; Peters, I. M. Technology and Market Perspective for Indoor Photovoltaic Cells. *Joule* **2019**, *3*, 1415−1426.

(8) Michaels, H.; Rinderle, M.; Freitag, R.; Benesperi, I.; Edvinsson, T.; Socher, R.; Gagliardi, A.; Freitag, M. Dye-Sensitized Solar Cells under Ambient Light Powering Machine Learning: Towards Autonomous Smart Sensors for the Internet of Things. *Chem. Sci.* **2020**, *11*, 2895−2906.

(9) Yan, N.; Zhao, C.; You, S.; Zhang, Y.; Li, W. Recent progress of thin-film photovoltaics for indoor application. *Chin. Chem. Lett.* **2020**, *31*, 643−653.

(10) Snaith, H. J. Estimating the Maximum Attainable Efficiency in Dye-Sensitized Solar Cells. *Adv. Funct. Mater.* **2010**, *20*, 13−19.

(11) Higashino, T.; Imahori, H. Porphyrins as excellent dyes for dye-sensitized solar cells: Recent developments and insights. *Dalt. Trans.* **2015**, *44*, 448−463.

(12) Ji, J. M.; Zhou, H.; Eom, Y. K.; Kim, C. H.; Kim, H. K. 14.2% Efficiency Dye-Sensitized Solar Cells by Co-Sensitizing Novel Thieno[3,2-b]indole-Based Organic Dyes with a Promising Porphyrin Sensitizer. *Adv. Energy Mater.* **2020**, *10*, 2000124−2000112.

(13) Green, M. A.; Dunlop, E. D.; Hohl-Ebinger, J.; Yoshita, M.; Kopidakis, N.; Hao, X. Solar Cell Efficiency Tables (Version 56). *Progr. Photovolt.: Res. Appl.* **2020**, *28*, 629−638.
(14) Frank, A. J.; Kopidakis, N.; Van de Lagemaat, J. Electrons in Nanostructured TiO_2 Solar Cells: Transport, Recombination and Photovoltaic Properties. *Coord. Chem. Rev.* **2004**, *248*, 1165−1179.
(15) Manthou, V. S.; Pefkianakis, E. K.; Falaras, P.; Vougioukalakis, G. C. Co-Adsorbents: A Key Component in Efficient and Robust Dye-Sensitized Solar Cells. *ChemSusChem* **2015**, *8*, 588−599.
(16) Neale, N. R.; Kopidakis, N.; Van de Lagemaat, J.; Grätzel, M.; Frank, A. J. Effect of a Coadsorbent on the Performance of Dye-Sensitized TiO_2 Solar Cells: Shielding versus Band-Edge Movement. *J. Phys. Chem. B* **2005**, *109*, 23183−23189.
(17) Kay, A.; Graetzel, M. Artificial Photosynthesis. 1. Photosensitization of TiO_2 Solar Cells with Chlorophyll Derivatives and Related Natural Porphyrins. *J. Phys. Chem.* **1993**, *97*, 6272−6277.
(18) Lee, K. M.; Chen, C. Y.; Wu, S. J.; Chen, S. C.; Wu, C. G. Surface Passivation: The Effects of CDCA Co-Adsorbent and Dye Bath Solvent on the Durability of Dye-Sensitized Solar Cells. *Sol. Energy Mater. Sol. Cells* **2013**, *108*, 70−77.
(19) Salvatori, P.; Marotta, G.; Cinti, A.; Anselmi, C.; Mosconi, E.; De Angelis, F. Supramolecular Interactions of Chenodeoxycholic Acid Increase the Efficiency of Dye-Sensitized Solar Cells Based on a Cobalt Electrolyte. *J. Phys. Chem. C* **2013**, *117*, 3874−3887.
(20) Friedrich, D.; Valldecabres, L.; Kunst, M.; Moehl, T.; Zakeeruddin, S. M.; Grätzel, M. Dye Regeneration Dynamics by Electron Donors on Mesoscopic TiO_2 Films. *J. Phys. Chem. C* **2014**, *118*, 3420−3425.
(21) Trilaksana, H.; Shearer, C.; Kloo, L.; Andersson, G. G. Restructuring of Dye Layers in Dye Sensitized Solar Cells: Cooperative Adsorption of N719 and Chenodeoxycholic Acid on Titania. *ACS Appl. Energy Mater.* **2019**, *2*, 124−130.
(22) Liu, W.; Jiang, H.; Shi, J.; Lu, B.; Cai, H.; Mao, Z.; Kong, F. In Situ Evaluation of Kinetics and Interaction Mechanism between Chenodeoxycholic Acid and N719 on Dye-Sensitized Nanofilm Surface. *ACS Appl. Energy Mater.* **2020**, *3*, 3310−3317.
(23) Hofmann, A. F.; Hagey, L. R. Key Discoveries in Bile Acid Chemistry and Biology and Their Clinical Applications: History of the Last Eight Decades. *J. Lipid Res.* **2014**, *55*, 1553−1595.
(24) Lee, Y. G.; Park, S.; Cho, W.; Son, T.; Sudhagar, P.; Jung, J. H.; Wooh, S.; Char, K.; Kang, Y. S. Effective Passivation of Nanostructured TiO_2 Interfaces with PEG-Based Oligomeric Coadsorbents to Improve the Performance of Dye-Sensitized Solar Cells. *J. Phys. Chem. C* **2012**, *116*, 6770−6777.
(25) Lee, Y. G.; Song, D.; Jung, J. H.; Wooh, S.; Park, S.; Cho, W.; Wei, W.; Char, K.; Kang, Y. S. TiO_2 Surface Engineering with Multifunctional Oligomeric Polystyrene Coadsorbent for Dye-Sensitized Solar Cells. *RSC Adv.* **2015**, *5*, 68413−68419.
(26) An, H.; Song, D.; Lee, J.; Kang, E. M.; Jaworski, J.; Kim, J. M.; Kang, Y. S. Promotion of Strongly Anchored Dyes on the Surface of Titania by Tetraethyl Orthosilicate Treatment for Enhanced Solar Cell Performance. *J. Mater. Chem. A* **2014**, *2*, 2250−2255.
(27) Park, S. H.; Lim, J.; Song, I. Y.; Atmakuri, N.; Song, S.; Kwon, Y. S.; Choi, J. M.; Park, T. Stable Dye-Sensitized Solar Cells by Encapsulation of N719-Sensitized TiO_2 Electrodes Using Surface-Induced Cross-Linking Polymerization. *Adv. Energy Mater.* **2012**, *2*, 219−224.
(28) Abreu, C. M. R.; Fonseca, A. C.; Rocha, N. M. P.; Guthrie, J. T.; Serra, A. C.; Coelho, J. F. J. Poly(vinyl chloride) by reversible deactivation radical polymerization: current status and future perspectives. *Prog. Polym. Sci.* **2018**, *87*, 34−69.
(29) Perrier, S. 50th Anniversary Perspective: RAFT Polymerization - A User Guide. *Macromolecules* **2017**, *50*, 7433−7447.
(30) Hora, C.; Santos, F.; Sales, M. G. F.; Ivanou, D.; Mendes, A. Dye-Sensitized Solar Cells for Efficient Solar and Artificial Light Conversion. *ACS Sustainable Chem. Eng.* **2019**, *7*, 13464−13470.
(31) Qi, F. Y.; Huang, Q. Y.; Jiao, F.; Zheng, Y. Z.; Gan, Y. C.; Xie, J. Characterization of N719 Dye Desorption on TiO_2 Nanotube Arrays Used for Dye-Sensitized Solar Cells. *Adv. Mater. Res.* **2013**, *631-632*, 524−529.
(32) Singh, J.; Gusain, A.; Saxena, V.; Chauhan, A. K.; Veerender, P.; Koiry, S. P.; Jha, P.; Jain, A.; Aswal, D. K.; Gupta, S. K. XPS, UV-Vis, FTIR, and EXAFS Studies to Investigate the Binding Mechanism of N719 Dye onto Oxalic Acid Treated TiO_2 and Its Implication on Photovoltaic Properties. *J. Phys. Chem. C* **2013**, *117*, 21096−21104.
(33) Schiffmann, F.; Vandevondele, J.; Hutter, J.; Wirz, R.; Urakawa, A.; Baiker, A. Protonation-Dependent Binding of Ruthenium Bipyridyl Complexes to the Anatase(101) Surface. *J. Phys. Chem. C* **2010**, *114*, 8398−8404.
(34) Ferwerda, R.; Van Der Maas, J. H.; Van Duijneveldt, F. B. Pyridine Adsorption onto Metal Oxides: An Ab Initio Study of Model Systems. *J. Mol. Catal. A: Chem.* **1996**, *104*, 319−328.
(35) Wei, L.; Yang, Y.; Fan, R.; Wang, P.; Dong, Y.; Zhou, W.; Luan, T. Enhance the Performance of Co-Sensitized Solar Cell by a Series Efficient Pyridine-Anchor Co-Adsorbents of N,N′-Bis((Pyridin-2-yl)methylene)-p-Phenylenediimine and a Ruthenium Dye of N719. *J. Power Sources* **2015**, *293*, 203−212.
(36) Connor, P. A.; Dobson, K. D.; McQuillan, A. J. Infrared Spectroscopy of the TiO_2/Aqueous Solution Interface. *Langmuir* **1999**, *15*, 2402−2408.
(37) León, A.; Reuquen, P.; Garín, C.; Segura, R.; Vargas, P.; Zapata, P.; Orihuela, P. FTIR and Raman Characterization of TiO_2 Nanoparticles Coated with Polyethylene Glycol as Carrier for 2-Methoxyestradiol. *Appl. Sci.* **2017**, *7*, 1−9.
(38) Panov, V. P.; Kazarin, L. A.; Dubrovin, V. I.; Gusev, V. I.; Kirsh, Y. É. Infrared spectra of atactic poly-4-vinylpyridine. *J. Appl. Spectrosc.* **1974**, *21*, 1504−1510.
(39) Zaki, M. I.; Hasan, M. A.; Al-Sagheer, F. A.; Pasupulety, L. In Situ FTIR Spectra of Pyridine Adsorbed on SiO_2-Al_2O_3, TiO_2, ZrO_2 and CeO_2: General Considerations for the Identification of Acid Sites on Surfaces of Finely Divided Metal Oxides. *Colloids Surfaces A Physicochem. Eng. Asp.* **2001**, *190*, 261−274.
(40) Bezrodna, T.; Puchkovska, G.; Shimanovska, V.; Chashechnikova, I.; Khalyavka, T.; Baran, J. Pyridine-TiO_2 Surface Interaction as a Probe for Surface Active Centers Analysis. *Appl. Surf. Sci.* **2003**, *214*, 222−231.
(41) Akacem, Y.; Kassab, E. Vibrational Analysis of Pyridine Adsorption on the Brønsted Acid Sites of Zeolites Based on Density Functional Cluster Calculations. *J. Phys. Chem. C* **2008**, *112*, 19045−19054.
(42) Marwa, B. M.; Bruno, S.; Mongi, B.; Tran Van, F.; Abdelmottaleb, B. L. Modeling of Adsorption Isotherms of Dye N719 on Titanium Oxide Using the Grand Canonical Ensemble in Statistical Physics for Dye Sensitized Solar Cells. *Sol. Energy* **2016**, *135*, 177−187.
(43) Gao, B.; Kong, D.; Zhang, Y. Preparation and Catalytic Activity of P4VP-Cu(II) Complex Supported on Silica Gel. *J. Mol. Catal. A: Chem.* **2008**, *286*, 143−148.
(44) Drelinkiewicz, A.; Hasik, M.; Quillard, S.; Paluszkiewicz, C. Infrared and Raman Studies of Palladium - Nitrogen-Containing Polymers Interactions. *J. Mol. Struct.* **1999**, *511-512*, 205−215.
(45) Zheng, T.; Zhu, M.; Waqas, M.; Umair, A.; Zaheer, M.; Yang, J.; Duan, X.; Li, L. P4VP-Ru^{II}(Bda) Polyelectrolyte-Metal Complex as Water Oxidation Catalyst: On the Unique Slow-Diffusion and Multi-Charge Effects of the Polyelectrolyte Ligand. *RSC Adv.* **2018**, *8*, 38818−38830.
(46) Harima, Y.; Fujita, T.; Kano, Y.; Imae, I.; Komaguchi, K.; Ooyama, Y.; Ohshita, J. Lewis-Acid Sites of TiO_2 Surface for Adsorption of Organic Dye Having Pyridyl Group as Anchoring Unit. *J. Phys. Chem. C* **2013**, *117*, 16364−16370.
(47) Lee, K. E.; Gomez, M. A.; Elouatik, S.; Demopoulos, G. P. Further Understanding of the Adsorption Mechanism of N719 Sensitizer on Anatase TiO_2 Films for DSSC Applications Using Vibrational Spectroscopy and Confocal Raman Imaging. *Langmuir* **2010**, *26*, 9575−9583.
(48) Sanzaro, S.; Fazio, E.; Neri, F.; Smecca, E.; Bongiorno, C.; Mannino, G.; Puglisi, R. A.; La Magna, A.; Alberti, A. Pervasive

https://doi.org/10.1021/acssuschemeng.1c00842
ACS Sustainable Chem. Eng. 2021, 9, 5981−5990

Infiltration and Multi-Branch Chemisorption of N-719 Molecules into Newly Designed Spongy TiO_2 Layers Deposited by Gig-Lox Sputtering Processes. *J. Mater. Chem. A* **2017**, *5*, 25529−25538.
(49) Chen, C.-Y.; Jian, Z.-H.; Huang, S.-H.; Lee, K.-M.; Kao, M.-H.; Shen, C.-H.; Shieh, J.-M.; Wang, C.-L.; Chang, C.-W.; Lin, B.-Z.; Lin, C.-Y.; Chang, T.-K.; Chi, Y.; Chi, C.-Y.; Wang, W.-T.; Tai, Y.; Lu, M.-D.; Tung, Y.-L.; Chou, P.-T.; Wu, W.-T.; Chow, T.-J.; Chen, P.; Luo, X.-H.; Lee, Y.-L.; Wu, C.-C.; Chen, C.-M.; Yeh, C.-Y.; Fan, M.-S.; Peng, J.-D.; Ho, K.-C.; Liu, Y.-N.; Lee, H.-Y.; Chen, C.-Y.; Lin, H.-W.; Yen, C.-T.; Huang, Y.-C.; Tsao, C.-S.; Ting, Y.-C.; Wei, T.-C.; Wu, C.-G. Performance Characterization of Dye-Sensitized Photovoltaics under Indoor Lighting. *J. Phys. Chem. Lett.* **2017**, *8*, 1824−1830.
(50) Mahbuburrahman, M.; Chandradebnath, N.; Lee, J.-J. Electrochemical Impedance Spectroscopic Analysis of Sensitization-Based Solar Cells. *Isr. J. Chem.* **2015**, *55*, 990−1001.
(51) Li, F.; Jennings, J. R.; Mathews, N.; Wang, Q. Evolution of Charge Collection/Separation Efficiencies in Dye-Sensitized Solar Cells Upon Aging: A Case Study. *J. Electrochem. Soc.* **2011**, *158*, B1158−B1163.

https://doi.org/10.1021/acssuschemeng.1c00842
ACS Sustainable Chem. Eng. 2021, 9, 5981−5990